Astronomy & Astrophysics manuscript no. paper_sub
June 26, 2014

Dynamics of a Multi-Thermal Loop in the Solar Corona

G. Nisticò[1], S. Anfinogentov[2], and V. M. Nakariakov[1,3,4]

[1] Centre for Fusion, Space and Astrophysics, Department of Physics, University of Warwick, CV4 7AL, UK e-mail: g.nistico@warwick.ac.uk
[2] Institute of Solar-Terrestrial Physics, Russian Academy of Science, Siberian Branch, 126a Lermontov st., 664033, Irkutsk, Russia e-mail: anfinogentov@iszf.irk.ru
[3] Central Astronomical Observatory at Pulkovo of the Russian Academy of Sciences, St Petersburg 196140, Russia
[4] School of Space Research, Kyung Hee University, Yongin, 446-701, Gyeonggi, Korea

Received June 26, 2014/Accepted dd mm yyyy

ABSTRACT

Context. We present an observation of a long-living **multi-thermal** coronal loop, visible in different EUV wavebands of SDO/AIA in a quiet-Sun region close to the Western solar limb.
Aims. Analysis of persistent kink displacements of the loop seen in different bandpasses that correspond to different temperatures of the plasma allows to reveal fine, sub-resolution structuring of the loop.
Methods. A vertically oriented slit is taken at the loop top and time-distance maps **are** made from it. Loop displacements in time-distance maps are automatically tracked with the Gaussian fitting technique and fitted with a "guessed" sinusoidal function. Wavelet transform are further used in order to quantify the periodicity variation in time of the kink oscillations.
Results. The loop strands are found to oscillate with the periods ranging between 3–**15** minutes. The oscillations are observed in intermittent regime with changes of the period and phase in time. The oscillations are different at three analysed wavelengths.
Conclusions. This finding suggests that the loop-like threads seen at different wavelengths are not co-spatial, and hence that the loop consists of several multi-thermal strands. The detected irregularity of the oscillation can be associated with a stochastic driver acting at the footpoints of the loop.

Key words. Sun: corona - Sun: oscillations - methods: observational

1. Introduction

Observations of the Sun at Extreme Ultra-Violet and X-Ray wavelengths have well shown that the solar corona is structured in the form of 1D curvilinear features, resembling closed loops in active regions, which outline the presence of strong magnetic field in the solar corona. These loops act as wave-guides for magnetohydrodynamic (MHD) waves. Theory of the propagation of MHD waves in a plasma cylinder has been formulated in seminal works of Zajtsev & Stepanov (1975); Roberts (1981); Roberts et al. (1984); Edwin & Roberts (1983), distinguishing between several different kinds of fast magnetoacoustic modes. Kink modes that are transverse displacements of the loop axis, were first observed with the Transition Region And Coronal Explorer (TRACE) mission (Aschwanden et al. 1999; Nakariakov et al. 1999). The following space missions as the Solar TErrestrial RElations Observatory (STEREO) and Hinode have permitted an intensive study of kink oscillations not only in coronal loops but also in prominence fibrils (e.g. Arregui et al. 2012), hot jets (Cirtain et al. 2007; Vasheghani Farahani et al. 2009), and post flare loops arcades (Verwichte et al. 2005). The fundamental mode, *i.e.* oscillations with nodes at the footpoints and an anti-node at the loop apex, polarised horizontally is mainly observed, but there is evidence of higher harmonics (Verwichte et al. 2004; De Moortel & Brady 2007) and vertically polarised oscillations (Wang & Solanki 2004; White et al. 2012). Kink oscillations of coronal loops, after being triggered by an impulsive event like a flare or a coronal mass ejection (CME), experience strong damping. Typically, the oscillations last for 3–4 periods only. Theoretical explanations of this damping has been addressed in term of "resonant absorption", *i.e.* conversion of the kink mode to a localised and hence invisible torsional Alfvén mode (Ruderman & Roberts 2002; Goossens et al. 2002, 2012).

Nowadays, the Solar Dynamics Observatory (SDO) space mission allows us to significantly improve our view of the Sun (Lemen et al. 2012). Thanks to the Atmospheric Imaging Assembly (SDO/AIA) **that is an array of 4 telescopes with 8 different filters, observing the solar corona at the highest temporal and spatial resolution possible today, a new regime of kink oscillations of coronal loops has been found**. Recently Nisticò et al. (2013a); Anfinogentov et al. (2013) detected "decay-less" kink oscillations. In this regime the oscillations do not experience damping. Moreover, these oscillations appear without any association with flares or CMEs. A signature of persistent kink oscillations has also been found in Wang et al. (2012) who described observations of growing kink oscillations of a coronal loop. The mechanism able to sustain the decay-less regime against the natural damping of kink waves is still unknown. There is also a need for quantifying the energy input that supports this mechanism. Thus, this new regime requires detailed observational study that would provide us with some hints for its understanding and interpretation.

In this paper, we analyse an example of irregular kink displacements of a **multi-thermal** coronal loop, observed in a quiet-Sun region simultaneously at three EUV wavelengths with SDO/AIA.

2. Observations

2.1. The **multi-thermal** *loop*

The coronal loop appeared on the south-western limb of the Sun in the field-of-view (FOV) of SDO/AIA on 21 January 2013 and was observed for almost 10 hrs. The loop had an approximately semi-circular shape. The loop was not associated with any active region. Fig. 1 shows a sequence of images demonstrating the temporal evolution of this loop at 171Å observed with SDO/AIA, and at 195Å with STEREO/EUVI-A.

The loop starts to light up in 171 Å around 14:10 UT (panel *a* of Fig. 1-left): it initially appears as a very thin semi-circular bright strip. Progressively, several rims appear subsequently above the previous one, and the intensity increases. The loop footpoints become very bright, resembling "flaring" (red circles in panel *b*). During the observations, several distinct loop bundles appear, experiencing some transverse displacements and intensity variation. The intensity variations can perhaps be attributed to the line-of-sight integration effect (Cooper et al. 2003). Also the external bundles are brighter than the internal ones, probably due to the same line-integration effect as the external bundles may have a bigger column-depth along the line-of-sight (panel *c*-*d*). At 20:20 UT, another loop appears behind, showing almost the same geometrical shape (green arrow in panel *e*). After 23:40 UT, the intensity progressively drops down and the loop disappears. **A movie showing the entire evolution of the loop (10 hrs, starting at 14:00 UT), in the same FOV as Fig. 1-left at 171 Å, with a cadence of 1 min, is provided in the online edition.**

The same region is visible from the Extreme Ultra-Violet Imager (EUVI) of the Solar TErrestrial RElations Observatory (STEREO)-A, showing another perspective of the loop, but the lower spatial and temporal resolution (1.6 arcsec, and 5 min at 195 Å) does not allow to capture the same details. Fig. 1-right shows a sequence of the same region at 195 Å, at the same time steps as in Fig. 1-left. It is possible to see the footpoints where the loop bundles are diverging from (red circle in panel *a*), but it is difficult to track them because of the low signal (the loop is enclosed in a dotted region in panels *b*-*c*).

The loop is also visible in other EUV bands with SDO/AIA, as seen in Fig. 2-top panel.

The detection of the loop in the other wavelengths could indicate that it is formed of multi-thermal elementary strands. What is possible to infer is that the footpoints are seen very well at hot temperatures (94, 131, 335 Å), whereas the loop body is more contrasted at "lower" temperatures (171, 193, 211 Å). It is not possible to immediately quantify what is the temperature of the loop/strands, because of the broad-band response in temperature of the AIA filters (for more details see Del Zanna 2013). The regularised inversion technique of Hannah & Kontar (2012) provides a method to get differential emission measures (DEMs) from AIA data (the code is provided at `http://www.astro.gla.ac.uk/~iain/demreg/`). We apply this technique to obtain DEM maps at several temperature intervals, ranging between 0.5–8 MK (Fig. 2-bottom panel), avoiding any formal discussion on the validity of the method. We simply show that the loop is apparently filled with low temperature plasma (0.5–1.5 MK) and, as temperatures increase, it becomes "fuzzier". The latter property has been largely studied in Guarrasi et al. (2010).

The overall structure of the loop appears as an "ensemble" of many diverging strands, probably organised in larger bundles, which share the same footpoints. The loop shape reflects the magnetic structure that can be inferred from extrapolation models as the Potential Field Source Surface (PFSS), where the magnetic field lines extrapolated from magnetograms are over plotted on the AIA 171 image (Fig. 3).

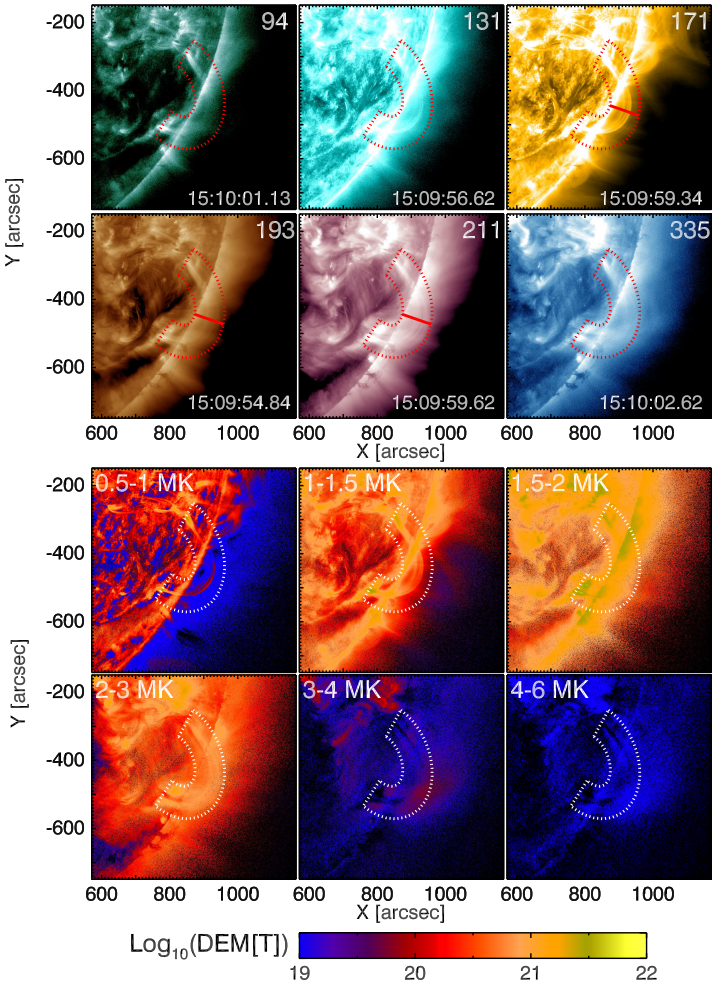

Fig. 2. Top: The loop at six EUV wavebands of SDO/AIA. From the left we have 94, 131, 171 Å (top row) and 193, 211, 335 Å(bottom row). Bottom: DEM maps of the studied region at different temperature ranges. In both panels, the loop is enclosed in a dotted region. The continuous line **located at the loop top at 171, 193, and 211 Å** marks the position of the slit.

2.2. 3D reconstruction

The geometry of the multi-thermal loop was reconstructed in the three-dimensional (3D) space by using the Principal Component Analysis (PCA). The details of the technique can be found in Nisticò et al. (2013b). Briefly, it provides an alternative method to fit a reasonable number of 3D points which sample the loop shape. It mainly consists of finding the typical eigenvalues and the corresponding eigenvectors of the covariance matrix of the 3D points, which will defines a set of three axes denoting a new reference frame related to the loop centre, as the normal to the loop plane, the major or minor axis of the ellipse which fits the loop shape. Other parameters such as the inclination and azimuth angles are retrieved geometrically from the orientation of this reference frame with respect the standard solar coordinate system.

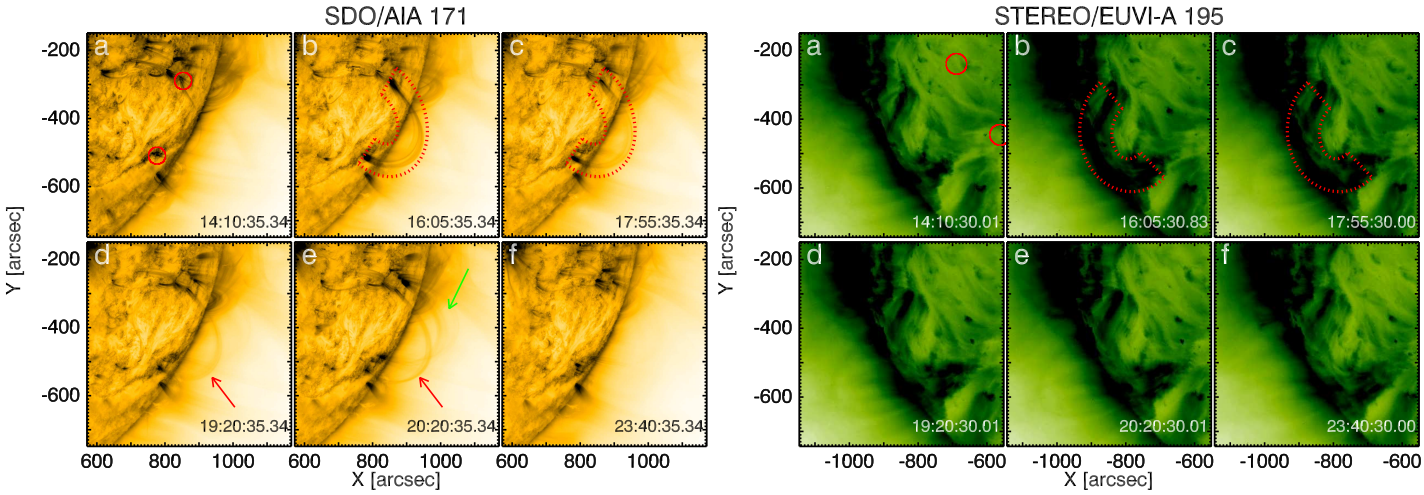

Fig. 1. Snapshots of the **multi-thermal** loop at several times, observed with SDO/AIA at 171 Å (left) and STEREO/EUVI-A at 195 Å (right). The circles mark the loop footpoints, whilst the dotted region ecloses the loop in both views. The red arrow mark the position of the loop during its evolution and the green one those of a transient loop in AIA. The temporal evolution as seen in the 171 Å channel of AIA (left panels) is available in the on-line edition.

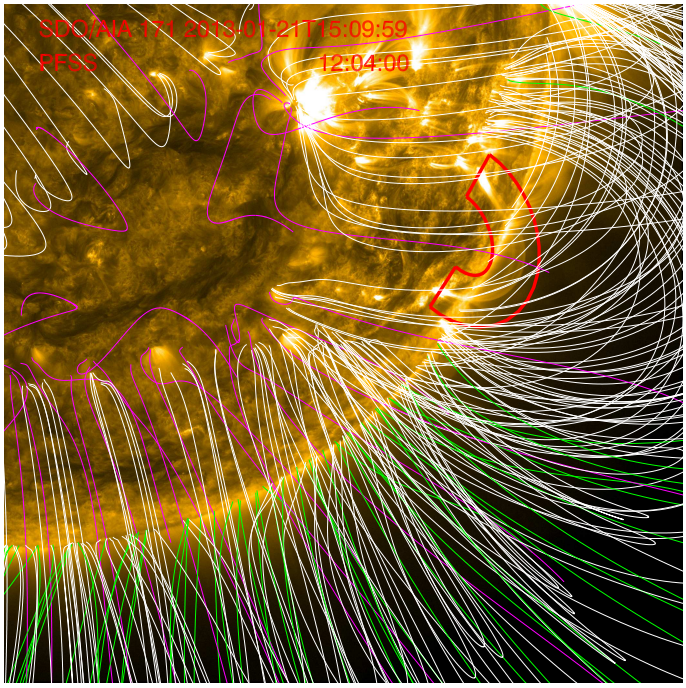

Fig. 3. SDO/AIA image at 171 Å **at about 15:10 UT** with PFSS extrapolated magnetic field lines over-plotted. **The PFSS model is referred to about 3 hrs before the AIA image**. The close magnetic field lines are marked in white, while the open magnetic field lines of positive polarity are in green and negative in purple.

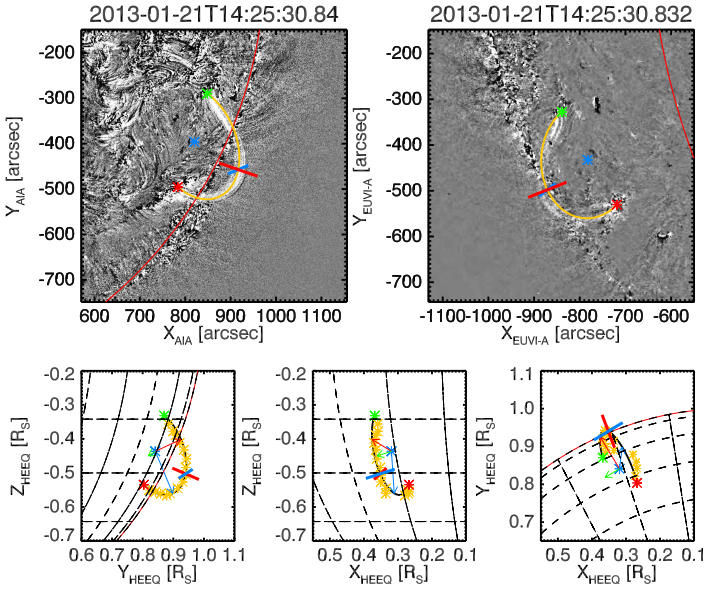

Fig. 4. **Top:** Geometry reconstruction of the loop in 3D **(yellow line)** using difference images of SDO/AIA 193 (top left) and STEREO/EUVI-A 195 (top right) views. **The northern loop footpoint is in green, whilst the southern one is in red, in blue the loop centre**. The vertical (red) and horizontal (blue) slit is over-plotted. Bottom: Projections of the loop in different orientations of the Heliocentric Earth Equatorial (HEEQ) coordinate system. Distance are expressed in solar radii (R_S) units. The 3D data points are plotted as yellow points and fitted by the black line. The green, red and blue arrows mark respectively the normal plane, the minor and major radius of the loop. The red and blue lines at the loop apex locate the vertical and horizontal slits.

The loop has almost a circular shape, since the minor and major radii, as deduced from the 3D reconstruction, are almost comparable, respectively, 0.107 and 0.136 $R_\odot$ (see Tab. 1 of Nisticò et al. 2013b). The loop is almost perpendicular to the solar surface since the estimated inclination is close to 0 deg (measured with respect to the radial direction out of the Sun), and it is mainly oriented along the North-South solar direction since the azimuth angle is about 73 deg. So, from the AIA perspective we can say the loop is almost perpendicular to the line of sight, since the loop centre is located at heliographic coordinates of (69.23,-25.88) deg, about 20 deg from the West solar limb. The loop has been reconstructed at a fixed time step that corresponded to the time about 14:25 UT. The loop shape does not seem to undergo significant changes during the time evolution of 10 hrs, except the local intensity variation of the loop bundles and small transverse motions around the equilibrium, and the solar rotation effects.

2.3. Data overview

In order to study transverse displacements of the loop, we downloaded FITS files at 171, 193, 211 Å, from 14:00 to 19:00 UT. Totally, we collected about 1500 frames for each wavelength, with a temporal cadence of 12 s and a spatial resolution of 0.6 arcsec. We extracted a subfield of 1000×1000 **pixels**, that represents the region-of-interest. We increased the signal-to-noise ratio of the images by constructing a running mean datacube, where each frame is the sum of 5 consecutive frames, corresponding to a time interval of 1 min: this allows to improve the quality of the images and keep the original temporal cadence. We took **a slit at the apex of the loop**, vertically and horizontally oriented (shown by the red and blue lines in Fig. 4, respectively). Since the vertical slit offer the best projection in the SDO/AIA field-of-view (FOV), we restrict our analysis on **it**. Starting from the vertical slit approximately located at the loop top, we build a time-distance map in order to depict transverse displacements.

3. Time-distance map analysis

In order to highlight the oscillatory patterns, we processed the time-distance (TD) maps by a "Laplacian" filter. The original time distance maps were convolved with a kernel that defines the uni-dimensional Laplacian operator:

$$\begin{pmatrix} 0 & -1 & 0 \\ 0 & 2 & 0 \\ 0 & -1 & 0 \end{pmatrix} \quad (1)$$

Th Laplacian operator defined in (1) is simply the second derivative along the vertical direction in the TD maps (hence the distance) and allows to highlight boundaries of the loop and preserve the time dimensions. The result of the convolution operation between the TD map and the kernel, is further smoothed with a Gaussian operator with a typical sigma of 1.5, in order to remove noise.

3.1. 171 Å

The filtered time-distance maps are given in Fig. 5 for 171, 193, and 211 Å. Bright patterns are clearly visible and outline the presence of **close** strands in the full loop structure, **which are separated from each other by less than 10 Mm**. We automatically track the position of the bright patterns in TD maps by fitting the intensity of each vertical slice with a Gaussian function: the maximum of the Gaussian locates the centre of the loop. Thus, time series of the loop displacements are obtained, and are over-plotted in red in the TD maps for the three wavelengths in Fig. 5.

The time series obtained from the 171 Å TD map are shown in the left column of Fig. 6. To remove the global trend of the time series (that can be due to long-period local variations or also the solar rotation) and highlight oscillation, we fit them with a **low-degree** polynomial functions (green lines). The "detrended" time series are plotted in the right column of Fig. 5. The oscillations are well depicted, but show relevant variations both in amplitude and period. The oscillations seems to be not stationary. This can be prove**d** by adapting some sine curves with specific period and amplitude just by an "eye-estimation" of the oscillations (colour lines in left column plots). The agreement between data and empirical sine curves is kept only at some time intervals, for a few cycles of the oscillation. Hence in different

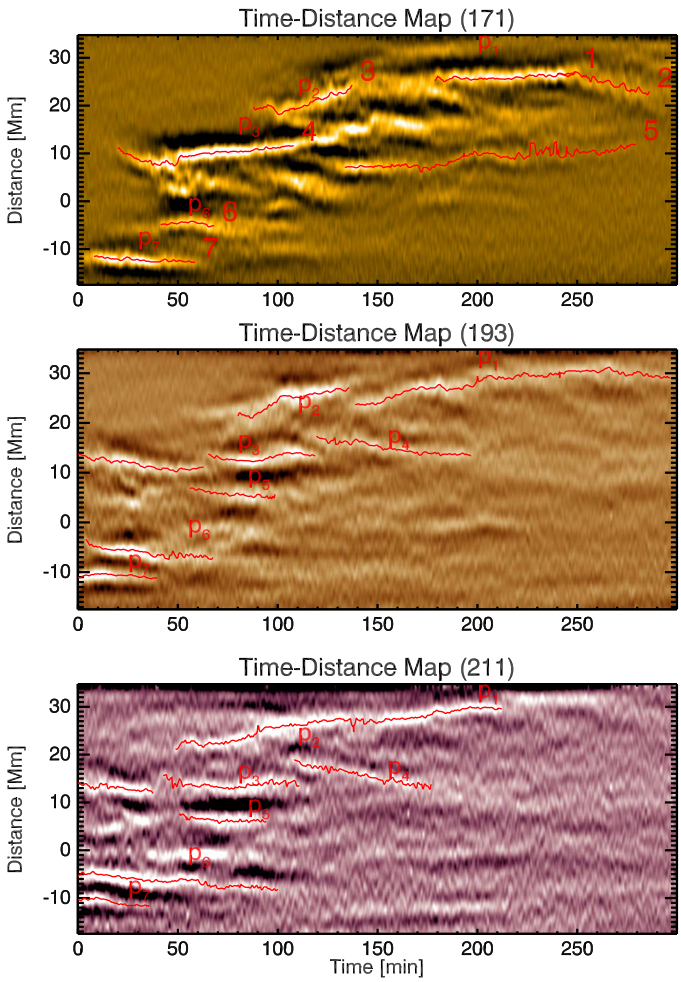

Fig. 5. Filtered time-distance maps at 171 (top), 193 (middle), and 211 Å (bottom). Oscillatory patterns obtained with an automatic Gaussian fitting are marked in red. The numbers shown are specifically related to the oscillatory patterns detected at 171 Å. **The series of labels "p"refers to some segments of the patterns extracted and compared between 171, 193 and 211 Å, which are simultaneous and apparently from the same geometrical locations.**

time intervals it is necessary to use a since curve with different parameters. This indicates that some external driver influences the loop oscillations, causing "intermittent" variation in amplitude and period. The values of the parameters of the sine curves **are** given in Table 1.

The extracted oscillations exhibit amplitudes close to the spatial resolution of the AIA pixel (*i.e.*∼0.435 Mm) ranging with values around 0.3–0.6 Mm, and some values smaller than 0.2 Mm. The reason of the sub-resolution estimation of the oscillation amplitude is due to the Gaussian fitting method, as pointed out also in Morton & McLaughlin (2013) using AIA and the High Resolution Coronal Imager (HI-C) data.

3.2. Wavelet analysis

As the observed transverse displacements of the loop are irregular in time, **a** more quantitative analysis can be done using the wavelet transform. The wavelet transform is often used in the analyses of time series with non-stationary power at different frequencies (Torrence & Compo 1998). Fig. 7 gives the global and

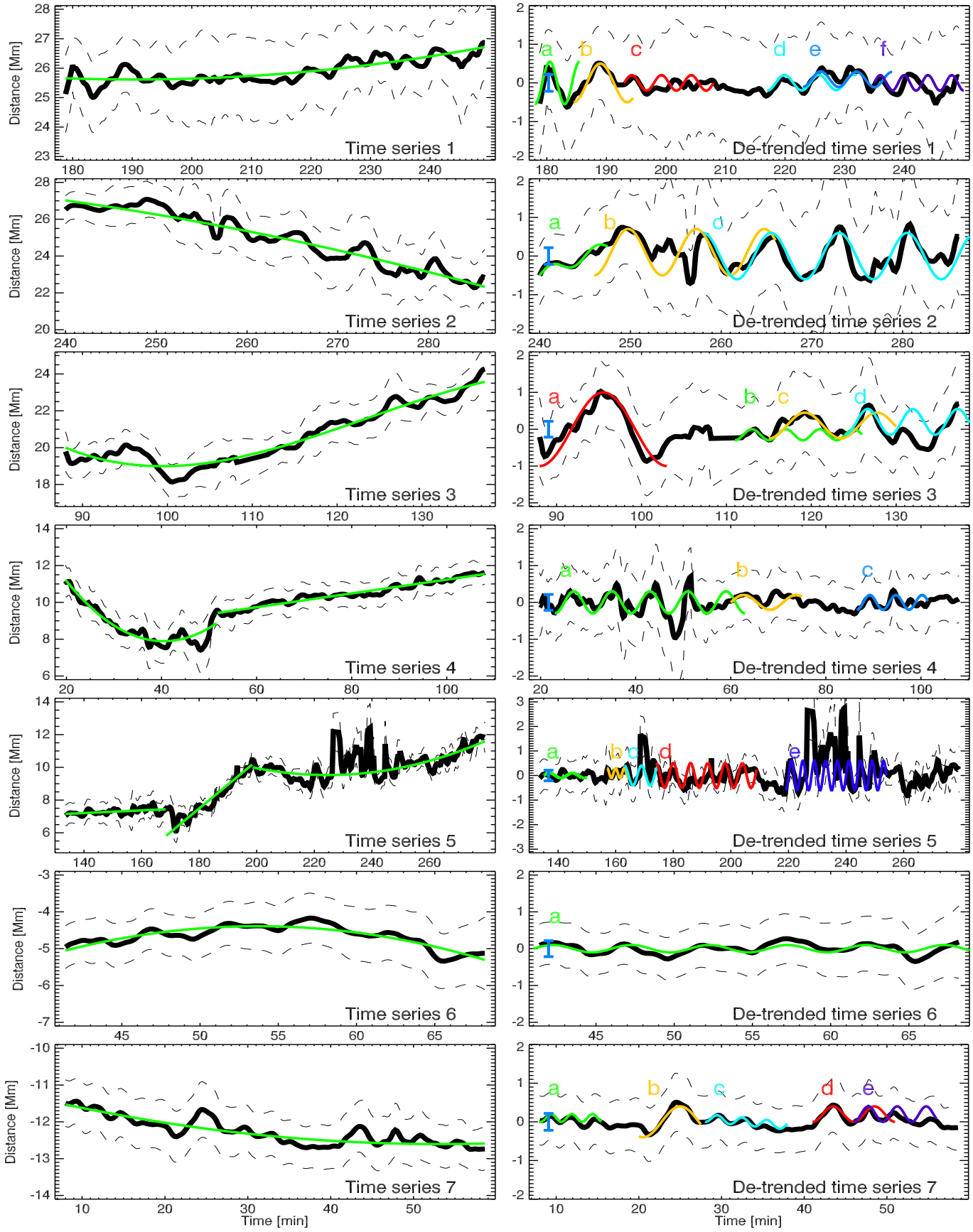

Fig. 6. Time series of the loop displacements extracted by a Gaussian fitting from the time distance map at 171 Å of Fig. 5. The original time series are shown on the left. The dashed lines outline the loop boundaries and are estimated from the σ of the Gaussian fitting. The overall series are fitted with a low-degree polynomial function (*i.e.* linear, quadratic, etc.) in order to determine their global trend, which has been removed in the left plots. A blue error bar in the right column of plots is shown in order to compare the amplitude of oscillations with the AIA spatial resolution (~ 0.4 Mm)

N_{oscill}	t_0 [min]	y_0 [Mm]	ξ [Mm]	P [min]	ϕ [deg]
Oscill (1)					
a	178.0	0.0	0.55	5.0	-180
b	184.5	0.0	0.50	9.0	-180
c	193.0	0.0	0.20	5.0	-90
d	217.0	0.0	0.20	5.8	-180
e	223.0	0.1	0.20	6.0	-180
f	235.0	0.0	0.20	4.0	-90
Oscill (2)					
a	240.0	-0.5	0.15	5.0	-90
b	246.5	0.1	0.60	9.0	-180
c	258.0	0.0	0.60	5.8	0
Oscill (3)					
a	88.0	0.0	1.0	15.0	-180
b	111.0	-0.3	0.15	4.0	-180
c	115.0	0.1	0.35	8.5	-180
d	124.0	0.2	0.35	5.3	-180
Oscill (4)					
a	23.0	0.0	0.30	8.0	-180
b	60.0	0.0	0.20	11.0	-90
c	86.5	0.0	0.20	5.5	-180
Oscill (5)					
a	135.0	0.0	0.10	8.0	-90
b	157.0	0.1	0.20	3.0	0
c	163.0	0.0	0.40	6.0	0
d	174.0	0.0	0.50	6.8	0
e	219.0	0.0	0.60	4.0	-180
Oscill (6)					
a	41.0	0.0	0.10	5.0	-90
Oscill (7)					
a	8.0	0.1	0.10	2.5	-200
b	20.0	0.0	0.40	9.0	-200
c	28.0	0.1	0.10	3.0	-180
d	41.0	0.0	0.20	5.0	-180
e	46.0	0.0	0.20	3.5	-180

Table 1. Parameters of the "eye" fittings of Fig. 6. Some segments of the oscillations are empirically fitted with a sinusoidal function, as $y = y_0 + \xi \cos(2\pi(t - t_0)/P + \phi)$, with y_0 the offset along the distance, t_0 the initial time oscillation interval, ξ, P and ϕ respectively the amplitude, period and phase of the oscillation. The related fittings are overlaid with different colours and labels (indicated in the first column) in Fig. 6.

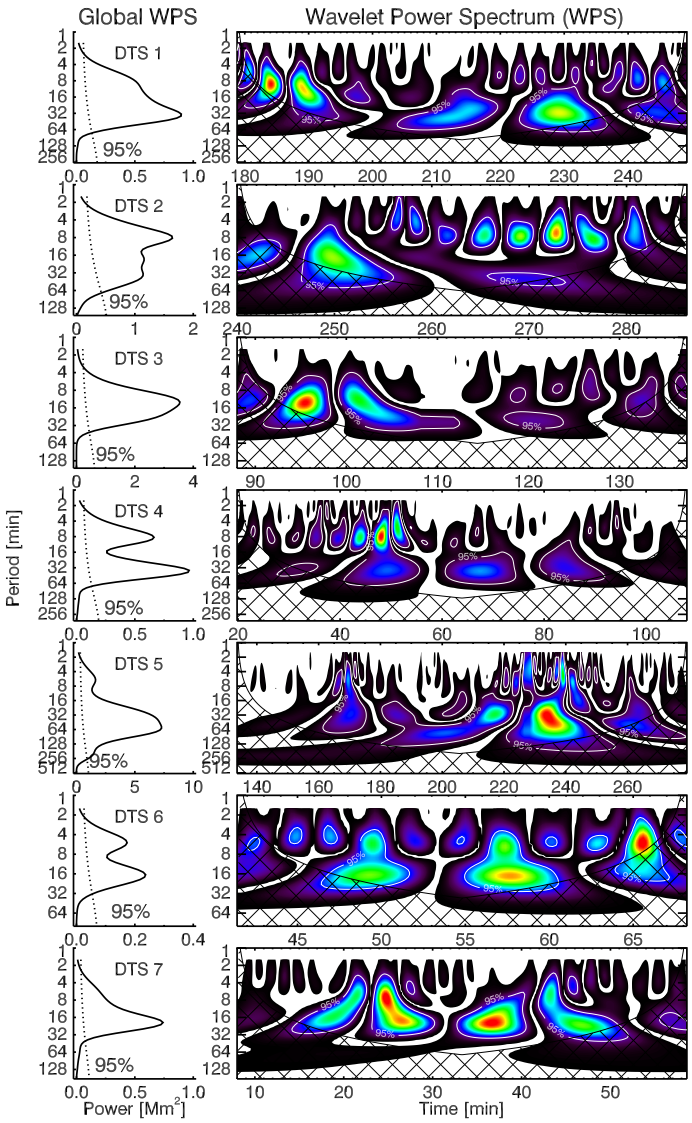

Fig. 7. Global (left) and time (right) wavelet power spectra of the de-trended time series (DTS) shown in Fig. 6.

time wavelet spectra of the de-trended time series shown in Fig. 6-right. The wavelet spectra are obtained by considering a second derivative of a Gaussian (*i.e.* the Mexican hat) as the mother wavelet, and the smallest scale of size 0.4 min (24 s). The global spectra reveal the presence of broad peaks and in some case of distinct peaks, which confirm the presence of the irregular oscillations in the time series. The majority of the 95% confidence levels fall in the region which is not affected by the cone of influence (cross-hatched lines). The periods range from 4 to 16 minutes.

3.3. Comparison of the 171, 193 and 211 Å oscillatory patterns

A comparison of the oscillatory patterns seen at the different wavelengths can provide additional information on the dynamics of the loop.

In Fig. 8 we plot a sequence of the oscillatory patterns seen at 171, 193, and 211 Å which share almost the same spatial location. The left column show the oscillations as obtained from the TD maps: these are independently de-trended with a polynomial function and plotted in the right column of Fig. 8. Subtracting different polynomials, every consistent with each oscillatory trend, should not introduce a major difference in the oscillations, since their time-scale are much longer than the period of the oscillations. On the other hand, from the original time-series, it is possible to notice that simultaneous oscillatory patterns, except for cases (d–e) for the 193Å and 211Å time series, do not share the same location and do not overlap in the TD maps: this indicates that different strands, possibly at different physical condition of temperature and density, contribute differently to each AIA filter. Moreover, the transverse displacements are not generally in phase, and because they are non-stationary displacements, they seem to response differently to a stochastic driver.

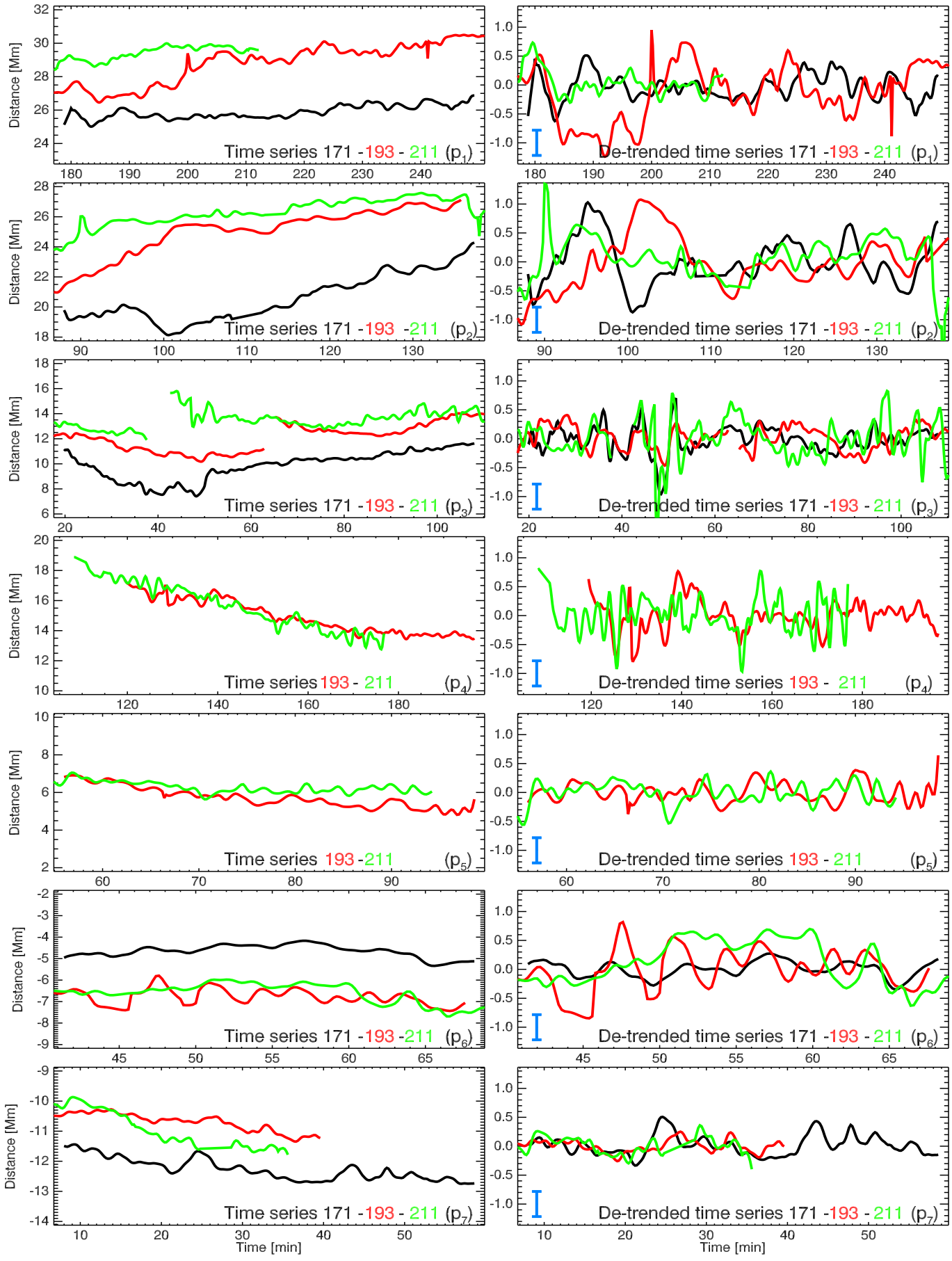

Fig. 8. Oscillatory patterns for the 171 (black), 193 (red), and 211 (green) Å obtained from the corresponding TD maps of Fig. **5**. Each time-series is independently de-trended by a low-degree polynomial function and shown in the right column of plots. The blue error bar on the left bottom corner shows the AIA pixel resolution equivalent to ~ 0.4 Mm.

4. Discussion and Conclusions

In this work we analysed the transverse oscillations of a coronal loop in a quiet-Sun region close to the solar limb, as observed from SDO/AIA, in order to study and provide new highlights on the decay-less kink oscillation observed from Wang et al. (2012); Nisticò et al. (2013a); Anfinogentov et al. (2013). The analysed loop was a rather peculiar, as it was well isolated from other loops, was not associated with a specific active region, and was visible simultaneously in different EUV wavelengths. **Our** findings can be summarised as follows:

1. The loop geometry has been reconstructed in 3D from SDO/AIA-193 and STEREO-A-195 views: we found that the loop can be modelled by an elliptical shape with a moderate eccentricity (the major axis is just 1.27 times larger the minor one, so that the loop is almost circular). The plane of the loop is almost perpendicular to the solar surface and it has a large azimuthal angle. The inspection of the AIA frames at several filters show that the loop is possibly constituted of finer strands, probably at different physical condition of density and temperature, as shown in the temperature analysis.
2. A time-distance map constructed from a slit located almost at the apex of the loop in the vertical (to the solar surface) direction, shows the presence of small-amplitude kink oscillations, comparable with the AIA spatial resolution. The oscillations, analysed at 171 Å, are automatically tracked with a Gaussian fitting technique and de-trended with a background polynomial function. They show some irregular variation of the period and amplitude. Only some certain time intervals can be "visually" fitted by a sinusoidal function with a constant period and amplitude. Wavelet power spectra show broad peaks in the range 4–16 min, with some drifts associated with the variations of the oscillation period and/or amplitude.
3. The comparison of oscillatory patterns simultaneously detected at 171, 193, and 211 Å show that they do not overlay in TD maps. It can be attributed to the fact that the loops seen in different bandpasses belong possibly to different strands that have different physical condition (temperature, density). Moreover the de-trended oscillations detected in different bandpasses are globally not in phase, having different periods and amplitudes.

The observed quasi-periodic transverse displacement of the multi-thermal loop makes its behaviour rather different from previously observed in coronal loops. Indeed, in contrast with the results obtained in the present study, the decay-less transverse oscillations previously detected in EUV loops were rather regular and monochromatic. The discrepancy can be possibly attributed to more effective damping of the oscillations in this loop. Consider kink oscillations of a coronal loop in terms of the empirical model suggested in Nisticò et al. (2013a). In this model the loop oscillations are described by a harmonic damped oscillator forced by an external driver. Assume that the driving force is random, representing, e.g., random granulation flows affecting the loop footpoints, or random flows in the corona. If the damping term in not too strong, the oscillations have a frequency close to the natural frequency of the oscillator, i.e. the frequency of the global kink mode. But, if the damping term is very strong, the oscillation follows the time pattern of the external driver. Hence perhaps what we see as the transverse displacements is the induced solution - the loop displacements forced by the irregular driver. Definitely, this interpretation is entirely speculative, and better understanding of this process requires a dedicated theoretical study, as well as an investigation on the techniques to extract loop displacement measurements near the detection threshold.

The clearly different displacement patterns seen in different bandpasses that are associated with the different temperatures of the emitting plasma can possibly be attributed to the unresolved fine structuring. The threads of different temperature have similar geometrical properties, but may have different physical properties. Thus, they may be affected by the external driver differently, showing different transverse displacement. The idea of the fine multi-thermal structuring of EUV coronal loops has already been employed in the previous multi-wavelength studies of MHD oscillations (King et al. 2003, e.g.). We would like to stress that the nature of the external driver of the kink displacements is not known and should be subject to follow-up research.

This interpretation seems to be consistent with the previously made assumption that kink oscillations in the multi-thermal loop are subject to more effective damping. Indeed, in the resonant absorption theory the energy of collective kink oscillations goes to the unresolved torsional motions at a narrow resonant shell (Ruderman & Roberts 2002; Goossens et al. 2002, 2012). If the analysed loop is a bundle of multi-thermal threads, there can be many resonant layers in its cross-section. Hence, in this multi-thermal loop the area of the resonant layers can be bigger than in usual mono-thermal loops, that would increase the efficiency of resonant absorption of kink oscillations.

Acknowledgements. Data are courtesy of the SDO/AIA and STEREO/SECCHI teams. This work is supported by the STFC, the Marie Curie PIRSES-GA-2011-295272 RadioSun project, the European Research Council under the SeismoSun Research Project No. 321141, the Russian Foundation of Basic Research under grant 13-02-00044, and the BK21 plus program through the National Research Foundation funded by the Ministry of Education of Korea.

References

Anfinogentov, S. A., Nisticò, G., & Nakariakov, V. M. 2013, A&A, 000, 000
Arregui, I., Oliver, R., & Ballester, J. L. 2012, Living Reviews in Solar Physics, 9, 2
Aschwanden, M. J., Fletcher, L., Schrijver, C. J., & Alexander, D. 1999, ApJ, 520, 880
Cirtain, J. W., Golub, L., Lundquist, L., et al. 2007, Science, 318, 1580
Cooper, F. C., Nakariakov, V. M., & Tsiklauri, D. 2003, A&A, 397, 765
De Moortel, I. & Brady, C. S. 2007, ApJ, 664, 1210
Del Zanna, G. 2013, A&A, 558, A73
Edwin, P. M. & Roberts, B. 1983, Sol. Phys., 88, 179
Goossens, M., Andries, J., & Aschwanden, M. J. 2002, A&A, 394, L39
Goossens, M., Andries, J., Soler, R., et al. 2012, ApJ, 753, 111
Guarrasi, M., Reale, F., & Peres, G. 2010, ApJ, 719, 576
Hannah, I. G. & Kontar, E. P. 2012, A&A, 539, A146
King, D. B., Nakariakov, V. M., Deluca, E. E., Golub, L., & McClements, K. G. 2003, A&A, 404, L1
Lemen, J. R., Title, A. M., Akin, D. J., et al. 2012, Sol. Phys., 275, 17
Morton, R. J. & McLaughlin, J. A. 2013, A&A, 553, L10
Nakariakov, V. M., Ofman, L., Deluca, E. E., Roberts, B., & Davila, J. M. 1999, Science, 285, 862
Nisticò, G., Nakariakov, V. M., & Verwichte, E. 2013a, A&A, 552, A57
Nisticò, G., Verwichte, E., & Nakariakov, V. M. 2013b, Entropy, 15, 4520
Roberts, B. 1981, Sol. Phys., 69, 27
Roberts, B., Edwin, P. M., & Benz, A. O. 1984, ApJ, 279, 857
Ruderman, M. S. & Roberts, B. 2002, ApJ, 577, 475
Torrence, C. & Compo, G. P. 1998, Bulletin of the American Meteorological Society, 79, 61
Vasheghani Farahani, S., Van Doorsselaere, T., Verwichte, E., & Nakariakov, V. M. 2009, A&A, 498, L29
Verwichte, E., Nakariakov, V. M., & Cooper, F. C. 2005, A&A, 430, L65
Verwichte, E., Nakariakov, V. M., Ofman, L., & Deluca, E. E. 2004, Sol. Phys., 223, 77
Wang, T., Ofman, L., Davila, J. M., & Su, Y. 2012, ApJ, 751, L27
Wang, T. J. & Solanki, S. K. 2004, A&A, 421, L33
White, R. S., Verwichte, E., & Foullon, C. 2012, A&A, 545, A129
Zajtsev, V. V. & Stepanov, A. V. 1975, Issledovaniia Geomagnetizmu Aeronomii i Fizike Solntsa, 37, 3